Molecular Therapy
Oncology
Original Article

# Oncolytic virus V937 in combination with PD-1 blockade therapy to target immunologically quiescent liver and colorectal cancer

Thai Q. Tran,[1] Jeff Grein,[2] Mohammed Selman,[1] Lakshmanan Annamalai,[2] Jennifer H. Yearley,[2] Wendy M. Blumenschein,[2] Svetlana Sadekova,[1] Alissa A. Chackerian,[1] Uyen Phan,[1] and Janica C. Wong[1]

[1]Discovery Oncology, Merck & Co., Inc, South San Francisco, CA 94080, USA; [2]Quantitative Biosciences, Merck & Co., Inc, South San Francisco, CA 94080, USA

**V937 is an investigational, genetically unmodified Kuykendall strain of coxsackievirus A21, which has been evaluated in the clinic for advanced solid tumor malignancies. V937 specifically infects and lyses tumor cells that overexpress intercellular adhesion molecule-1 (ICAM-1). Intratumoral V937 as a monotherapy and in combination with anti-PD-1 antibody pembrolizumab has shown clinical response in patients with metastatic melanoma, which overexpresses ICAM-1. Here, we investigate in preclinical studies the potential bidirectional cross-talk between hepatocellular carcinomas (HCC) or colorectal carcinomas (CRC) and immune cells when treated with V937 alone or in combination with pembrolizumab. We show that while V937 treatment of tumor cell lines or organoids or peripheral blood mononuclear cells (PBMCs) alone induced a minimal immunological response, V937 treatment of non-contact co-cultures of tumor cell lines or CRC organoids with PBMCs led to robust production of proinflammatory cytokines and immune cell activation. In addition, both recombinant interferon-gamma and pembrolizumab increased ICAM-1 on tumor cell lines or organoids and, in turn, amplified V937-mediated oncolysis and immunogenicity. These findings provide critical mechanistic insights on the cross-talk between V937-mediated oncolysis and immune responses, demonstrating the therapeutic potential of V937 in combination with PD-1 blockade to treat immunologically quiescent cancers.**

## INTRODUCTION

Immune checkpoint inhibitors have revolutionized the landscape of cancer treatment and significantly improved the clinical outcome for multiple cancer types, including non-small cell lung cancer and advanced melanoma.[1,2] Inhibition of the programmed cell death protein-1 (PD-1) unleashes a sustainable and durable antitumor response in T cells. However, clinical responsiveness to PD-1/PD-L1 blockade is primarily characterized by tumor cohorts containing a high density of tumor-infiltrating lymphocytes (TILs) and abundant tumor antigenic mutations.[3,4] A key strategy to increase sensitivity to immune checkpoint blockade is to develop therapeutics that recruit TILs and inflame immunologically quiescent tumors. Oncolytic viruses represent a versatile, immunotherapeutic modality that couples oncolysis of tumor cells with induction of antitumor innate and adaptive immune responses.[5–8] Virus-induced oncolysis can cause dying cancer cells to release tumor-associated antigens and both pathogen-associated molecular patterns (PAMPs) and cell-derived damage-associated molecular patterns (DAMPs) that serve as "danger signals" to prime the immune system.[9,10] The sensing of PAMPs/DAMPs by pattern recognition receptors, including Toll-like receptors (TLRs) and nucleotide-binding oligomerization domain-like receptors (NLRs), trigger the release of proinflammatory cytokines, chemokines, and type I interferons along with activation of antigen-presenting cells (APCs) and migration to lymph nodes, where they engage the adaptive immune system and activate antigen-specific T cells.[11–14] Clinical proof of concept has been achieved with Imlygic, talimogene laherparepvec (T-VEC), a genetically engineered herpes simplex virus type-1 (HSV-1) that expresses granulocyte-macrophage colony-stimulating factor (GM-CSF). Imlygic was approved by the US Food and Drug Administration in 2015 for intralesional treatment of advanced melanoma.[15]

V937 is an oncolytic, genetically unmodified Kuykendall strain of Coxsackievirus A21, a single-stranded RNA-positive enterovirus of the Picornaviridae family. The two critical components of V937 mechanism of action are the exploitation of differences between normal and malignant cells and the activation of host antitumor immunity. V937 binds to intercellular adhesion molecule-1 (ICAM-1), which is overexpressed on various tumor types and decay-accelerating factor (DAF).[16] ICAM-1 is required for V937 infection, and while V937 binding to DAF alone cannot initiate cell infection, DAF, a low-affinity receptor, facilitates high-affinity binding of V937 to ICAM-1.[16,17] Preclinical studies have shown that the high oncolytic activity of V937 in melanoma correlates with high cell surface expression of ICAM-1.[18] Furthermore, tumor cells are more permissive than normal cells to V937 viral replication due to their defects in antiviral interferon signaling.[18]

Received 19 July 2023; accepted 21 April 2024;
https://doi.org/10.1016/j.omton.2024.200807.

**Correspondence:** Svetlana Sadekova, Discovery Oncology, Merck & Co., Inc, South San Francisco, CA 94080, USA.
**E-mail:** svetlana.sadekova@merck.com

V937 has been tested in a number of clinical trials. Notably, in the Phase II CALM study to investigate the efficacy and safety of intratumoral V937 in patients with advanced melanoma, 38.6% (22 out of 57) of patients were responders (28.1% [16 out of 57] confirmed) based on immune-related Response Evaluation Criteria in Solid Tumors (irRECIST), and 21.1% (12 out of 57) had a durable response (maintenance of partial response or complete response [CR] per irRECIST for $\geq$6 months) lasting a median of 10.1 months (range, 5.8–14.8 months). In patients receiving $\geq$80% of scheduled injections, 27.5% (11 out of 40 patients) had a durable response lasting a median of 9.7 months (range, 5.8–14.8 months). Regression of melanoma was observed in non-injected lesions.[19] In the Phase 1b CAPRA single-arm trial of intratumoral V937 in combination with pembrolizumab in patients with advanced melanoma, the objective response rate was 47% (CR, 22%). Among 17 responders, 14 (82%) had responses $\geq$6 months.[20] Among eight patients previously treated with immunotherapy, three responded (one complete, two partial). Responses were associated with increased serum CXCL10 (IP-10) and CCL22, suggesting viral replication contributes to antitumor immunity. The clinical data provide added impetus to investigate V937 in combination with pembrolizumab to treat immunologically quiescent tumors.

In recent years, 3D organoid technology has revolutionized cancer modeling *in vitro*. Patient-derived organoids have been shown to be a relevant screening platform for oncolytic virus response and predictive of antitumor efficacy *in vivo*.[21–24] Three-dimensional culturing of organoids allows the expansion of heterogeneous cell types derived from primary patient tissues and preserves the physiologically relevant structure to overcome some of the intrinsic limitations of monolayer cell cultures. For example, the multicellular complexity of organoids permits a more relevant viral replication cycle and 3D structure for virus internalization and intracellular trafficking.[21,23,24] Here, we report using a co-culture system of tumor cell lines or colorectal carcinoma (CRC) organoids with immune cells to delineate the mechanism of action of V937 monotherapy as well as in combination with pembrolizumab.

## RESULTS

### Variable expression of cell surface ICAM-1 on melanoma, HCC, and CRC tissues

The surface expression of ICAM-1 on tumor cells and immune cells in formalin-fixed paraffin-embedded (FFPE) tissue samples of melanoma, hepatocellular carcinoma (HCC), and CRC was assessed by immunohistochemistry (Figures 1A–1C). Approximately 50% (45 out of 93) of the melanoma samples expressed ICAM-1 on greater than 50% of the tumor cells, and the percentage of ICAM-1+ cells was higher among tumor cells than among immune cells. In contrast, approximately 70% (46 out of 63) of the HCC samples expressed ICAM-1 on less than 50% of the tumor cells. But similar to the melanoma cohort, the percentage of ICAM-1+ cells in HCC samples was higher among tumor cells than among immune cells. For CRC samples ($n$ = 63), minimal to mild apical staining of ICAM-1 on tumor cells was often observed but was not scored in this study, as the expression on apical surfaces does not come in contact with blood or interstitial fluid and hence is not accessible by intratumorally or systemically dosed V937 (Figure 1C). In contrast, several human CRC cell lines have been reported to express ICAM-1.[25] However, it is important to note that CRC differs in the extent to which cellular polarity is retained, with some maintaining clear apical and basolateral surfaces, and others losing this distinction completely.[26] CRC cell lines expressing ICAM-1 could derive from tumors, which *in situ* might have retained apical distribution of expression, with circumferential redistribution of the protein occurring in the dissociated state. They may also result from tumors in which all tumor cell polarity has been lost. In contrast, we found no major difference in ICAM-1 expression in immune cells across the tumor types tested. Together, these results suggest that ICAM-1 expression in HCC and CRC tumor cells is lower than in melanoma.

### Oncolytic and immunogenic activity of V937 in HCC cell lines

The cell surface expression of ICAM-1 on a panel of human HCC cell lines was assessed by flow cytometry. Four out of the five tested HCC lines SNU-387, SNU-423, SNU-475, and SNU-449 were positive for ICAM-1, and SNU-182 was negative for ICAM-1 (Figure 2A). The five HCC cell lines were evaluated for their susceptibility to V937-mediated oncolysis. Cell viability was assessed 72 h following V937 infection at multiplicity of infection (MOI) = 0.0001, 0.001, 0.01, 0.1, 1, and 10. The ICAM-1+ cell lines were all susceptible to V937 oncolysis, whereas SNU-182 was not susceptible to V937 oncolysis (Figure 2B). The half maximal inhibitory concentrations (IC50s) for SNU-387, SNU-423, and SNU-475 were $\leq$0.1 MOI, and the IC50 for SNU-449 was at approximately MOI = 1. V937-induced oncolysis was evaluated with Incucyte Live-Cell Analysis. Dead cells were labeled with Incucyte Cytotox Green, which permeates unhealthy cells due to the perturbation in plasma membrane integrity. V937 induced dose-dependent cytotoxicity for SNU-423, SNU-449, but not in ICAM-1 low SNU-182 cell line (Figures 2C and S1A–S1C).

To elucidate the immunogenic activity of V937, non-contact cell culture of tumor cells and PBMCs was utilized. In brief, $5 \times 10^5$ cells of the HCC cell lines were seeded in six-well plates, and $2 \times 10^6$ PBMCs were seeded inside the hydrophilic polytetrafluoroethylene cell culture inserts with pore size of 0.4 μm. The three cell culture conditions for the assay were as follows: (1) HCC cells alone in the lower chamber, (2) PBMCs alone in the upper chamber, and (3) HCC cells in the lower chamber and PBMCs in the upper chamber. In triplicate ($n$ = 3), media (mock-treated) or V937 at MOI = 2 was added to the lower chamber. V937 is ∼28 nm and can pass from the lower chamber to the upper chamber through the 0.4-μm pores of the insert. The cell culture media was harvested following V937 treatment for 72 h and assayed for various cytokines and chemokines. As shown for SNU-475, V937 treatment of only the co-culture of SNU-475 cells and PBMCs resulted in significant induction of interferon (IFN)-α, interleukin (IL)-12, IFN-γ, IP-10, macrophage inflammatory protein (MIP)-1α, and IL-6 compared to mock-treated cultures (Figure 2D). It is important to note that when the cell cultures were mock-treated, the levels of some cytokines/chemokines were higher in the culture of PBMCs alone than in the co-culture of SNU-475 and PBMCs. It is

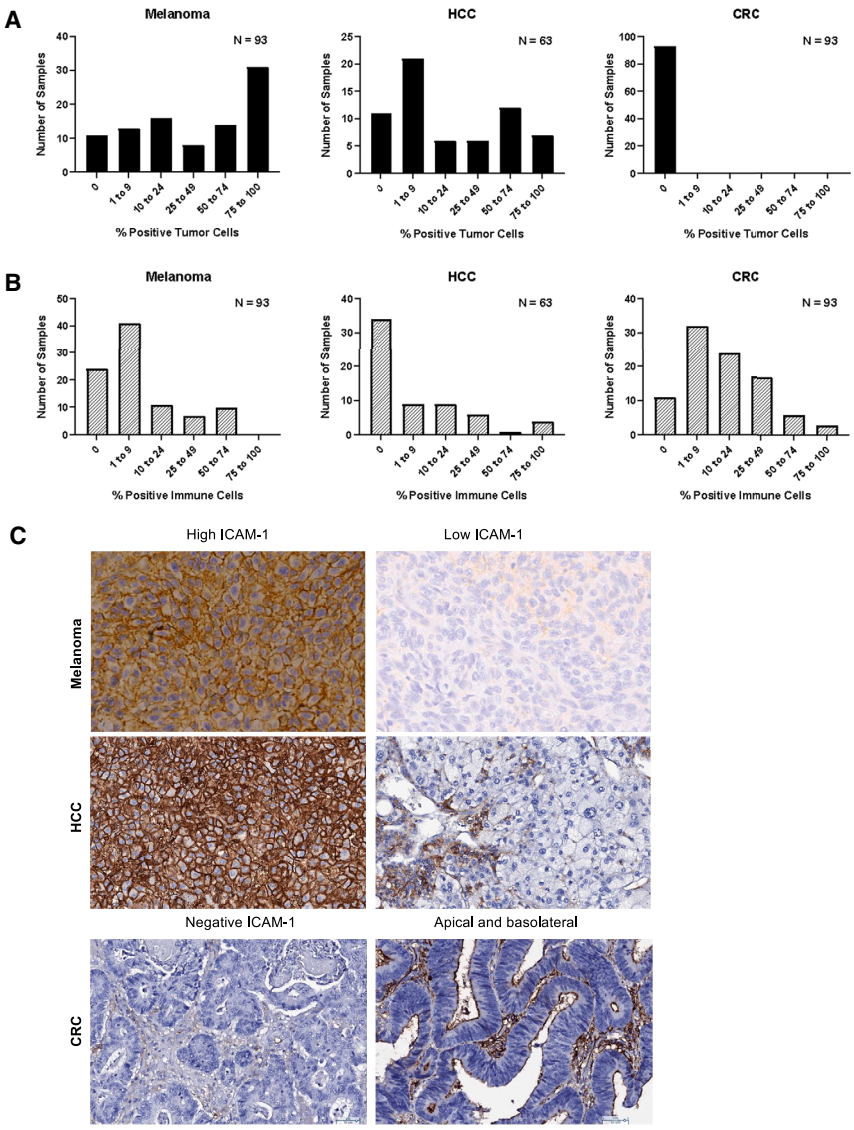


**Figure 1. Prevalence of ICAM-1+ tumor cells and immune cells in melanoma, HCC, and CRC tissues**

(A and B) Prevalence of ICAM-1+ tumor cells (A) and immune cells (B) in melanoma, HCC, and CRC tissues was assessed by immunohistochemistry. Samples were scored by a pathologist based on the frequency of positive cell expression, irrespective of staining intensity. The evaluated tissues were commercially sourced, FFPE specimens from the Merck Research Laboratories South San Francisco tissue bank: melanoma ($n = 93$), HCC ($n = 63$), and CRC ($n = 93$). (C) Representative IHC images of ICAM-1 staining in melanoma, HCC, and CRC tissues are shown. Scale bar, 50 μm.

hypothesized that secreted proteins by SNU-475 cells suppressed cytokine/chemokine production by PBMCs. Nevertheless, the data showed that even in the immunosuppressive environment created by the co-culture of tumor cells and immune cells, V937 treatment was able to induce an immune response in the PBMCs. Under the experimental conditions, V937 at MOI = 2 did not induce secretion of cytokines in the single culture of either the SNU-475 cells or PBMCs, demonstrating that V937's immunogenic effect on PBMCs was indirect and was linked to oncolysis of SNU-475 cells in the co-culture system. It is important to note that monocytes (CD14+) express ICAM-1.[17,27] As shown in Figure 1B, the immune cells in a portion of melanoma, HCC, and CRC FFPE specimens expressed ICAM-1. Therefore, V937 may also have a direct effect on PBMCs. Previously, it had been shown that V937 can directly induce induction of IFN-α in PBMCs.[17]

### Oncolytic and immunogenic activity of V937 in CRC cell lines

Similar studies were completed for a panel of CRC cell lines. CACO2, DLD1, and SW48 had moderate/high cell surface expression of ICAM-1. ICAM-1 expression was lower in HT29 and SW837 and very low/undetectable in NCI-H508 (Figure 3A). The six CRC cell lines were evaluated for their susceptibility to V937-mediated oncolysis. Cell viability was assessed 72 h following V937 infection at MOI = 0.0001, 0.001, 0.01, 0.1, 1, and 10. The oncolytic activity of V937 in CACO2, DLD1, and SW48 was low, with IC50s between 1 and 10 MOI, whereas V937 had little or no oncolytic activity in HT29, SW837, and NCI-H508 (Figure 3B). Furthermore, Incucyte Live-Cell Analysis was utilized to evaluate V937-induced oncolysis of ICAM-1+ CACO2 and ICAM-1-NCI-H508. Imaging at 72 h following V937 infection (MOI = 0.001, 0.01, 0.1, and 1) and labeling with Incucyte Cytotox Green dye showed moderate oncolysis in CACO2 and very low oncolysis in NCI-H508 (Figure 3C). Treatment of V937 at MOI = 2 of the non-contact co-culture of $5 \times 10^5$ CACO2 cells and $2 \times 10^6$ PBMCs resulted in significant induction of inflammatory cytokines IFN-α, IL-12, IFN-γ, IP-10, MIP-1α, and IL-6 (Figure 3D). Although V937 induced lower oncolysis in CACO2 than in SNU-475 (Figure 2B), V937 was able to induce a robust secretion of cytokines from PBMCs in co-culture of CACO2 and PBMCs.

### V937 induces oncolysis in CRC organoids

The organoid platform is a novel 3D culture recently shown to recapitulate tumor biology and heterogeneity of patients' tumors.[28–30] Importantly, recent studies have demonstrated the potential of tumor organoid cultures to predict clinical response to chemotherapeutic drugs.[31,32] Colorectal organoids were generated from resected CRC and normal adjacent tissues from CRC patients (Figure 4A). CRC organoid lines (CRC-2 and CRC-3) and one normal colorectal organoid line (NC-1) were generated by culturing dissociated tissues using the embedded

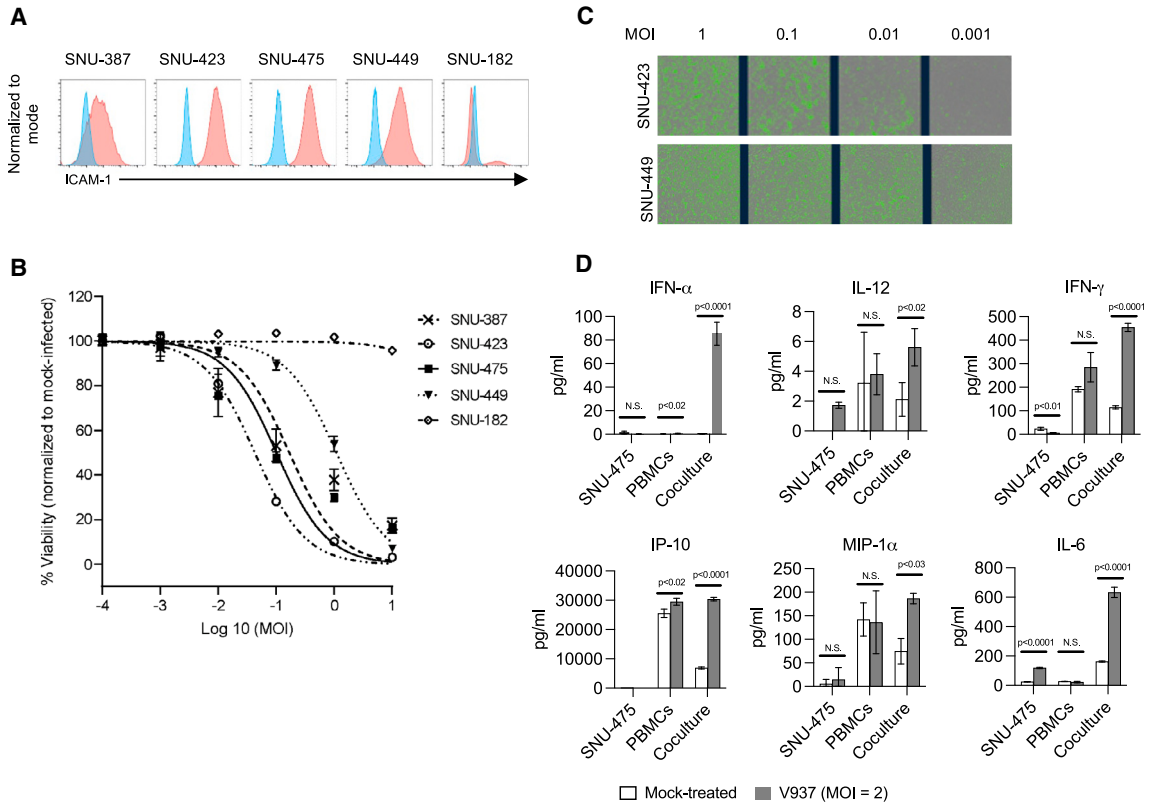


**Figure 2. Expression of ICAM-1 on HCC cell lines and susceptibility to V937 oncolytic and immunogenic activity**

(A) The cell surface expression of ICAM-1 on human HCC cell lines SNU-387, SNU-423, SNU-475, SNU-449, and SNU-182 was assessed by flow cytometry. Cells were incubated with either the relevant PE-conjugated isotype control antibody (blue histogram) or PE-conjugated anti-ICAM-1 monoclonal antibody (red histogram). (B) Cell viability of the five cell lines was determined 72 h following infection with V937 at MOI = 0.0001, 0.001, 0.01, 0.1, 1, and 10 ($n = 5$) in CellTiter-Glo 2.0 assay (Promega). Mean percentages of viability, normalized to mock-infected, ± standard deviations are shown. (C) Representative Incucyte Live-Cell images of SNU-423, SNU-449 cells, cultured at 37°C in Incucyte S3 IC50745 following V937 treatment at the indicated MOI and labeling with Incucyte Cytotox Green dye ($n = 3$) are shown. (D) The media from the single culture of SNU-475 cells ($5 \times 10^5$ cells) or PBMCs ($2 \times 10^6$ cells) or the co-culture of SNU-475 cells and PBMCs following mock or V937 (MOI = 2) treatment for 72 h were assayed for protein concentrations of various cytokines and chemokines using multiplexed electrochemiluminescent assays ($n = 3$). Mean ± standard deviations for IFN-α, IL-12, IFN-γ, IP-10, MIP-1α, and IL-6 are shown. Significant differences are indicated by the $p$ values when $p < 0.05$.

matrigel method.[33] Cell surface ICAM-1 expression of normal colon and CRC organoids were assessed by flow cytometry. The normal colon NC-1 organoids were negative for ICAM-1 expression, while CRC organoids were positive for ICAM-1 expression (Figures 4B and 4C, respectively). V937-induced oncolysis was then evaluated with Incucyte. We found that Annexin V was more sensitive in detecting cell death in organoids than Cytotox Green, based on the response of organoid CRC-2 treated with V937 (Figure S2A). This is likely due to lower basal cell death levels and a better signal-to-noise ratio with Annexin V staining. Imaging and quantitation of Incucyte Annexin V Red dye following V937 treatment showed that at MOI = 20, V937 induced minimal oncolysis in NC-1 organoids but significant oncolysis in both CRC-2 and CRC-3 organoids (Figures 4B, 4C, S2B, and S2C).

### Cross-talk between V937-infected CRC organoids and immune cells in non-contact co-culture

Similar to the studies with the HCC and CRC cell lines, the CRC organoids were evaluated in non-contact co-culture with PBMCs with approximately $5 \times 10^5$ cells of CRC organoids seeded in the lower chamber and $2 \times 10^6$ PBMCs seeded in the upper chamber. The three cell culture conditions for the assay were as follows: (1) CRC-2 organoids alone in the lower chamber, (2) PBMCs alone in the upper chamber, and (3) CRC-2 organoids in the lower chamber and PBMCs in the upper chamber. The various cell cultures were treated with V937 at MOI = 0 (mock-treated), 1, and 5, and 48 h following treatment, CRC-2 organoids, PBMCs, and culture medium were harvested. CRC-2 organoids and PBMCs were snap-frozen, and ribonucleic acid was isolated for analysis of ICAM-1, CVA21, and various immune gene expression. As shown for MOI = 5, co-culture of CRC-2 organoids and PBMCs resulted in an increase in ICAM-1 mRNA expression in the CRC-2 organoids even without V937 treatment (Figure 5A, left panel, open bars). This suggests that factors that were secreted by PBMCs induced ICAM-1 mRNA expression in the CRC-2 organoids. Interestingly, compared with the mock-treated, addition of V937 further increased ICAM-1 mRNA expression in the CRC-2 organoids in the co-culture with PBMCs (Figure 5A, left

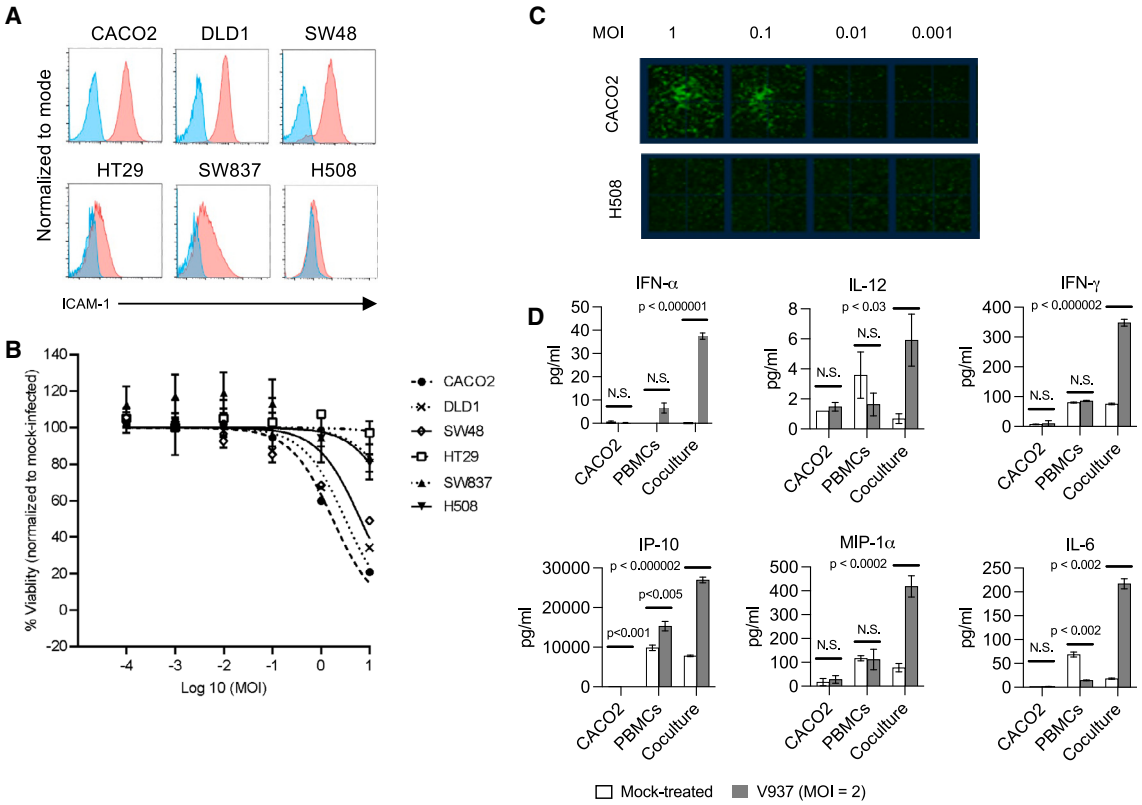


**Figure 3. Expression of ICAM-1 on CRC cell lines and susceptibility to V937 oncolytic and immunogenic activity**

(A) The cell surface expression of ICAM-1 on human CRC cell lines CACO2, DLD1, SW48, HT29, SW837, and NCI-H508 was assessed by flow cytometry. Cells were incubated with either the relevant PE-conjugated isotype control antibody (blue histogram) or PE-conjugated anti-ICAM-1 monoclonal antibody (red histogram). (B) Cell viability of the six cell lines was determined 72 h following infection with V937 at MOI = 0.0001, 0.001, 0.01, 0.1, 1, and 10 ($n = 5$) in CellTiter-Glo 2.0 assay (Promega). Mean percentages of viability, normalized to mock-infected, ± standard deviations are shown. (C) Representative Incucyte Live-Cell Analysis images of CACO2 and NCI-H508 cells, cultured at 37°C in Incucyte S3 IC50745 following 72 h of V937 treatment at MOI = 0.001, 0.01, 0.1, and 1 and labeling with Incucyte Cytotox Green dye ($n = 3$) are shown. (D) The media from the single culture of CACO2 cells ($5 \times 10^5$ cells) or PBMCs ($2 \times 10^6$ cells) or the co-culture of CACO2 cells and PBMCs following mock or V937 (MOI = 2) treatment for 72 h were assayed for protein concentrations of various cytokines and chemokines using multiplexed electro chemiluminescent assays ($n = 3$). Mean ± standard deviations for IFN-α, IL-12, IFN-γ, IP-10, MIP-1α, and IL-6 are shown. Significant differences are indicated by the $p$ values when $p < 0.05$.

panel, solid bars). In contrast, ICAM-1 mRNA expression in the PBMCs was comparable in the absence or presence of CRC-2 organoids, and V937 treatment did not increase ICAM-1 mRNA expression in the single culture of PBMCs or co-culture with CRC-2 organoids (Figure 5A, left panel). Compared with the single culture of CRC-2 organoids, V937 treatment resulted in approximately a 6-fold increase in CVA21 (V937) mRNA expression in CRC-2 organoids when co-cultured with PBMCs. In contrast, CVA21 mRNA expression in PBMCs cultured alone or with CRC-2 organoids following V937 treatment was comparable (Figure 5A, right panel). The data suggest bidirectional cross-talk in the co-culture system of CRC-2 organoids and PBMCs wherein V937-induced oncolysis of CRC-2 organoids resulted in activation of PBMCs. Factors secreted by PBMCs in turn increased ICAM-1 mRNA expression on CRC-2 organoids, leading to increased V937 infection, replication, and subsequently higher CVA21 mRNA expression in the CRC-2 organoids. For the mock-treated cultures, the mRNA expression of ICAM-1 was comparable between the single cultures of CRC-2 organoids and PBMCs. In contrast, CVA21 mRNA expression was 6-fold higher in the PBMCs than in the CRC-2 organoids. This suggests that V937 infection in PBMCs was more effective than in the CRC-2 organoids.

It has previously been shown that although V937 infects PBMCs, it does not induce robust oncolysis in PBMCs.[34] PBMCs are less permissible to V937 replication due to intact interferon signaling. Indeed, we showed that V937 infection of healthy donor PBMCs did not result in apoptosis as assessed by DNA fragmentation ELISA (Figure S3A). Analysis of gene expression in the PBMCs from single culture of PBMCs and co-culture of CRC-2 organoids and PBMCs showed that compared with mock-treated (MOI = 0), V937 at MOI = 1 or 5 induced at least 2-fold increase in many genes. These genes are critical in TLR signaling (TLR7, CD40, and CD80), NLR signaling (MEFV, PSTPIP1, CARD9), immune cell recruitment (CXCL6 and CXCR3), T cell mediated killing (GZMA, GZMB, IFN-γ), and regulating T cell activation (PD-1, LAG3) (Figure 5B). Furthermore, V937 induced apoptosis in ICAM-1-positive CRC-3

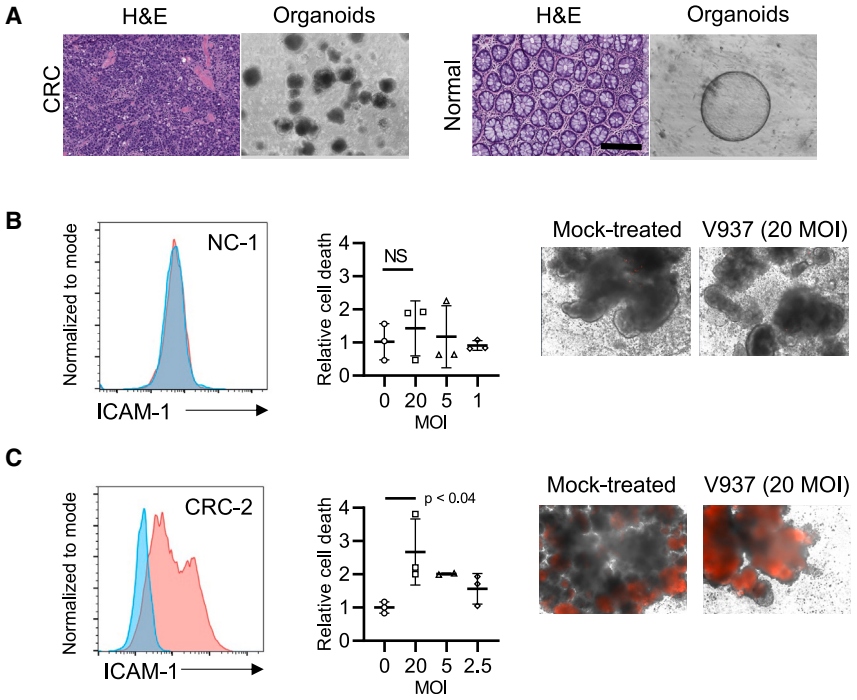


**Figure 4. V937 induces cell death in CRC organoids but not in normal colon organoids**

(A) Representative H&E images of CRC tumor tissue and normal colon tissue, scale bar, 200 μm (left) and brightfield images of the derived normal colon and CRC organoids are shown. Oncolytic activity of V937 in normal colon organoids (B) and CRC organoids (C) was assessed in Incucyte Live-Cell Analysis System. Normal colon organoids (NC-1) and CRC organoids (CRC-2) were treated with V937 at indicated MOI and labeled with Incucyte Annexin V Red dye. Cell surface expression of ICAM-1 on organoids are shown. Organoids were incubated with either the relevant PE-conjugated isotype control antibody (blue histogram) or PE-conjugated anti-ICAM-1 monoclonal antibody (red histogram). Quantitation of Annexin V Red dye (mean ± standard deviations) at 72 h following mock (MOI = 0) or V937 treatment (MOI at indicated MOI) and representative Incucyte Live-Cell Analysis images (mock-treated and MOI = 20) are shown. Significant differences are indicated by the *p* values when $p < 0.05$ (NS = not significant).

organoids. V937 treatment of the co-culture of CRC-3 organoids and PBMCs for 72 h resulted in induction of various immune genes in PBMCs (Figure S3B).

### IFN-γ induced ICAM-1 expression on cancer cells potentiates V937 oncolytic activity

ICAM-1 mRNA expression positively correlates with IFN-γ mRNA expression in primary CRCs (CRC primary tumors [$n = 288$], The Cancer Genome Atlas [TCGA] database) ($R = 0.63$, $p < 2.2e{-}16$) (Figure 5C). It is imperative to consider that ICAM-1 mRNA expression encompasses the sum of expression on the tumor cells and immune cells in the CRC tumors. It has previously been shown that recombinant IFN-γ induced ICAM-1 expression in head and neck squamous cell carcinoma (HNSCC) cell lines.[35] Subsequently, we showed that recombinant IFN-γ induced ICAM-1 expression in CRC cell line WIDR in a dose-dependent manner (Figure 5D). Furthermore, the effects of 0.01 ng/mL IFN-γ on V937-induced oncolysis of WIDR cells was evaluated using the Incucyte Live-Cell Analysis System. Quantitation of Incucyte Cytotox Green dye 72 h following V937 infection showed that IFN-γ increased oncolysis at all MOIs (0.2, 1, 5, and 20) (Figure 5E). Interestingly, V937 at MOI = 0.2 with 0.01 ng/mL IFN-γ induced comparable levels of oncolysis in WIDR cells to that induced by V937 at MOI = 20 without IFN-γ (Figure 5E).

### Pembrolizumab potentiates V937-induced oncolysis of CRC cell line and organoids

We tested whether activation of T cells with CD3 cross-linking and treatment with anti-PD-1 pembrolizumab mimic the effects of IFN-γ. In the presence of anti-CD3 mAb (5 ng/mL), single culture of COLO205 or co-culture of COLO205 and PBMCs were treated with either 10 μg/mL immunoglobulin (Ig)G4 isotype control, 10 μg/mL pembrolizumab, V937 (MOI = 5) + 10 μg/mL IgG4 isotype control, or V937 (MOI = 5) + 10 μg/mL pembrolizumab for 3 days. In the co-culture of COLO205 and PBMCs, the treatment with pembrolizumab induced cell surface ICAM-1 expression in ICAM-1 low COLO205 cell line (Figure 6A). Furthermore, V937 lysed COLO205 only when co-cultured with PBMCs and in the presence of pembrolizumab (Figure 6B). Analysis of the culture media showed that V937 in combination with pembrolizumab increased protein secretion of IFN-γ, IP-10, and IL-1β compared with treatment with V937 or pembrolizumab alone (Figure 6C). In contrast, V937 alone or in combination with pembrolizumab both induced secretion of IFN-α in the co-culture (Figure 6C). Similarly, in co-culture studies using CRC-3 organoids and PBMCs, treatment with V937 (5 MOI) in combination with pembrolizumab (10 μg/mL) and anti-CD3 (5 ng/mL) for 72 h resulted in significant oncolysis of CRC-3 organoids (Figure 6D). Representative brightfield images showed that the combination of V937 and pembrolizumab resulted in loss of integrity of the cell membranes of the CRC-3 organoids (Figure 6E).

### V937 sensitizes CRC tumors to anti-PD-1 therapy in CD34+ humanized mice

The antitumor efficacy of intratumorally administered V937 alone or in combination with pembrolizumab administered intraperitoneally, was evaluated in CRC-2 organoid-derived model using 20-week-old CD34+ humanized NSG mice (The Jackson Laboratory). The huCD34+ NSG mice were engrafted with human cord blood derived CD34+ cells from three immune donors, and all mice were confirmed to have engraftment of >25% hu-CD45+ cells in the peripheral blood. CRC-2 organoids ($2 \times 10^6$ cells) were subcutaneously injected in flanks of the huCD34+ NSG mice ($n = 40$). Treatment was initiated

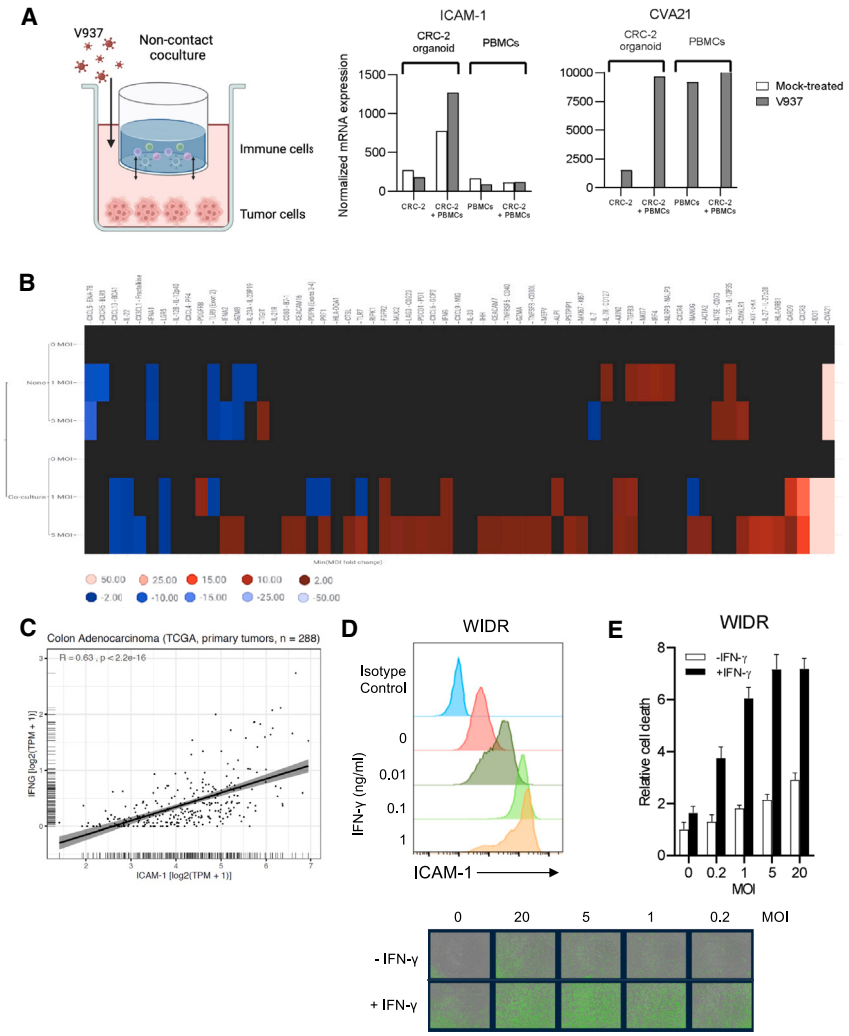


**Figure 5. IFN-γ induced ICAM-1 expression on CRC tumors potentiates V937-mediated oncolysis**

(A) Fluidigm qPCR analysis for various genes on RNA isolated from CRC-2 organoids ($5 \times 10^5$ cells) or PBMCs ($2 \times 10^6$ cells) in single culture or co-culture, mock-treated, or treated with V937 (MOI = 1 and 5) for 48 h were completed. mRNA expression of genes was normalized to ubiquitin. A visual representation of the non-contact co-culture is shown. Normalized mRNA levels of CVA21 (V937 RNA) (left) and ICAM-1 on CRC-2 organoid and PBMCs from the single culture of co-culture, mock-treated or treated with V937 (MOI = 5) for 48 h are shown. (B) Heatmap of fold-change of genes with greater than 2-fold increase or decrease over mock-treated following V937 treatment at MOI = 1 and 5 of PBMC single culture or non-contact co-culture of CRC-2 and PBMCs is shown. (C) Spearman correlation depicting regression line with confidence intervals between mRNA expression of IFN-γ and ICAM-1 in CRC primary tumors ($n$ = 288) (TCGA database) is shown; R = 0.63, $p < 2.2e{-}16$. (D) Following treatment with recombinant human IFN-γ (0.01, 0.1, and 1 ng/mL) for 24 h, cell surface expression of ICAM-1 on CRC cell line WIDR was assessed by flow cytometry. Staining with PE-conjugated isotype control antibody (blue histogram) is shown for untreated WIDR cells and staining with PE-conjugated anti-ICAM-1 monoclonal antibody is shown for untreated and IFN-γ treated cells. (E) In the presence of absence of 0.01 ng/mL IFN-γ, WIDR cells were mock-treated or treated with V937 (MOI = 0.2, 1, 5, and 20) for 72 h and labeled with Incucyte Cytotox Green dye ($n$ = 3). Cell death was normalized to condition with no addition of IFN-γ or V937. Mean ± standard deviations are shown.

when the mean tumor volume reached 80 $mm^3$ 2 weeks following implantation of CRC-2 organoids. The mice, representing three immune donors, were distributed across four groups: Group 1: PBS/IgG4 isotype control; Group 2: V937; Group 3: pembrolizumab; and Group 4: V937 + pembrolizumab. Immunohistochemical (IHC) analysis of tumors that were collected on day 42 post-implantation confirmed that implanted CRC-2 organoids expressed ICAM-1 (Figure 7A). PBS and V937 ($10^8$ plaque-forming units [PFU]) were administered intratumorally on days 0, 2, 4, 6, 13, 17, and 20, and human IgG4 control mAb and pembrolizumab (10 mg/kg) were administered intraperitoneally on days 0, 7, and 14. Compared with treatment with V937 or pembrolizumab alone, V937 in combination with pembrolizumab resulted in a significant reduction in tumor burden of subcutaneous CRC-2 organoids (Figures 7B and 7C).

## DISCUSSION

V937 in combination with pembrolizumab was investigated in the clinic to evaluate the safety, tolerability, and efficacy in patients with melanoma, non-small cell lung cancer, and bladder cancer (NCT02043665, NCT04521621). While the treatment regimen has a manageable safety profile, the clinical responses in early trials were also reported to be varied among tumor types.[19,36] These tumor cohorts have variable ICAM-1 expression levels, which may affect response to V937. Therefore, preclinical studies to elucidate the mechanism of action of V937 in combination with PD-1 blockade in other tumor types of solid tumors may provide important insights for using V937 as a therapeutic agent.

In the present study, we showed that oncolysis of V937 was dependent on ICAM-1 expression on the tumor cell lines. V937 induced robust oncolysis in ICAM-1-positive HCC cell lines and no oncolysis in the ICAM-1 negative HCC cell line. Similarly, V937 induced modest oncolysis in CRC cell lines that expressed robust levels of ICAM-1 but not in cell lines with no ICAM-1 expression. V937-induced oncolysis in cancer cells alone did not result in induction of cytokines and chemokines in the tumor cell lines themselves, nor did V937 induce the secretion of cytokines and chemokines from PBMCs. However, V937 treatment of the non-contact co-culture of both SNU-475 and CACO2 with PBMCs resulted in the induction

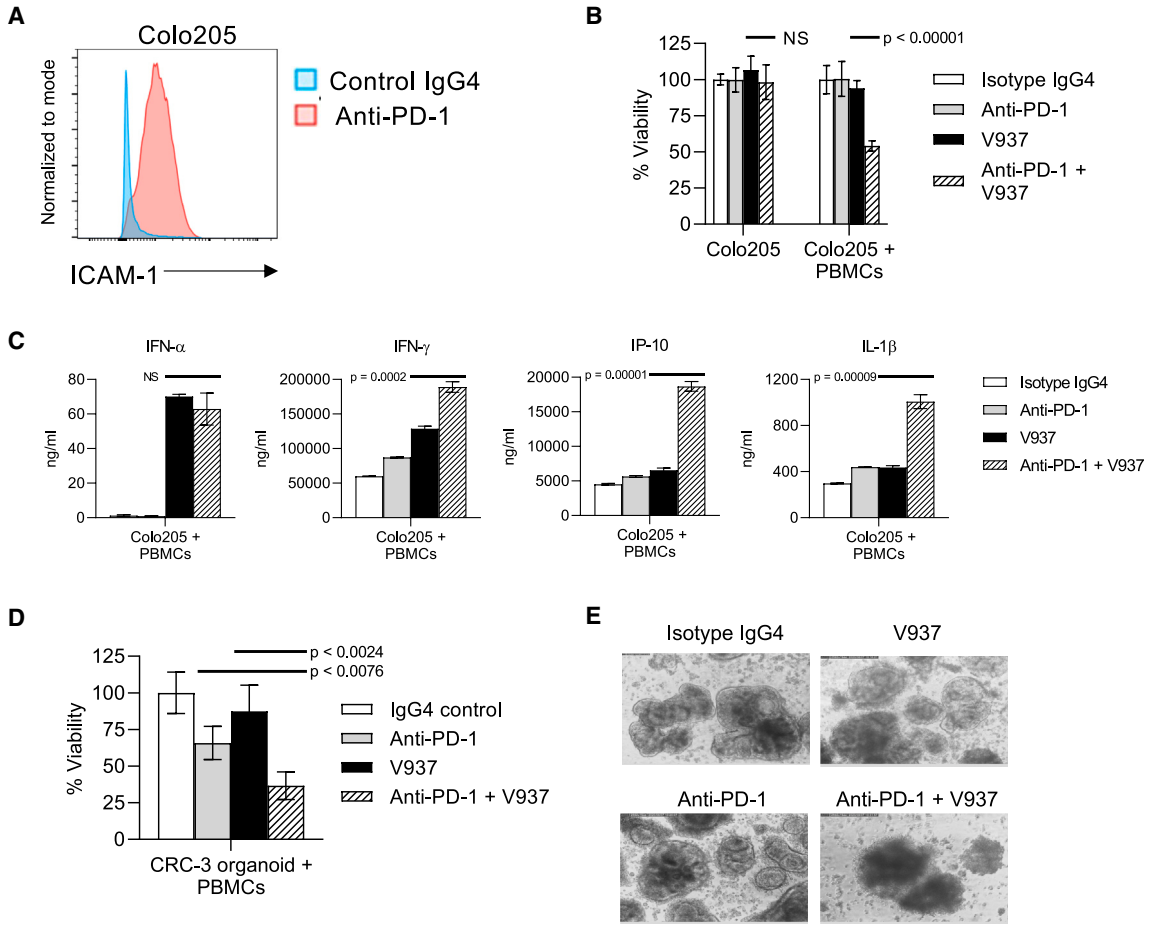


**Figure 6. Anti-PD-1 treatment of co-culture of CRC cell line or organoid with PBMCs potentiate V937-induced oncolysis**

(A) Induction of ICAM-1 expression in COLO205 in a non-contact co-culture system with PBMCs upon anti-PD-1 antibody treatment in the presence of 5 ng/mL anti-CD3 for 72 h. (B) COLO205 or co-culture of COLO205 and PBMCs, in presence of anti-CD3 mAb (5 ng/mL) was treated with either IgG4 isotype control (10 μg/mL), anti-PD-1 pembrolizumab (10 μg/mL), V937 (MOI = 5), and pembrolizumab (10 μg/mL) + V937 (MOI = 5) ($n$ = 4) for 72 h at 37°C, 5% $CO_2$. Cell viability of COLO205 was determined in CellTiter-Glo 2.0 assay (Promega). Mean percentages of viability, normalized to Ig4 isotype control-treated, ± standard deviations are shown. $p$ values between V937 and anti-PD-1 + V937 groups are shown; significant differences are indicated by the $p$ values when $p < 0.05$ (NS = not significant). (C) The media from the co-culture of COLO205 cells and PBMCs with the various treatments were harvested at 72 h and assayed for protein concentrations of various cytokines and chemokines using multiplexed electrochemiluminescence-based assays ($n$ = 3). Mean ± standard deviations for IFN-α, IFN-γ, IP-10, and IL-1β are shown. $p$ values between V937 and anti-PD-1 + V937 groups are shown; significant differences are indicated by the $p$ values when $p < 0.05$. (D) Cell viability was assessed in CRC-3 organoids in CellTiter-Glo 2.0 assay following treatment of the co-culture of CRC-3 organoids and PBMCs, in presence of anti-CD3 (5 ng/mL), with either IgG4 isotype control (10 μg/mL), anti-PD-1 pembrolizumab (10 μg/mL), V937 (MOI = 5), and pembrolizumab (10 μg/mL) + V937 (MOI = 5) for 72 h at 37°C, 5% $CO_2$ ($n$ = 4). Significant differences are indicated by the $p$ values when $p < 0.05$. (E) Representative brightfield images of CRC-3 organoids from the co-culture with PBMCs at 72 h under the treatment of IgG4 isotype control, V937 (MOI = 5), pembrolizumab (10 μg/mL), V937 (MOI = 5), and pembrolizumab (10 μg/mL) + V937 (MOI = 5), all treatment groups included the presence of anti-CD3 mAb (5 ng/mL).

of cytokines IFN-α, IL-12, IFN-γ, IL-6, and chemokines IP-10 and MIP-1α. The induction of the cytokines and chemokines only in the co-culture reflects the dependency of immune activation on V937-induced oncolysis.

Patient-derived organoids have been utilized to evaluate lytic and antitumor activity of various oncolytic viruses including adenovirus and measles vaccine virus.[22–24] Here, we evaluated not only the lytic activity of V937 in patient-derived CRC organoids and normal colon organoids, but also assessed how V937-induced oncolysis may activate immune cells. We showed that V937 treatment resulted in oncolysis of ICAM-1+ CRC-2 organoids and did not kill normal organoids. In co-culture of CRC-2 organoids and PBMCs, V937 activated genes that were critical in both innate and adaptive immune responses. V937-mediated activation of both innate and adaptive immunity demonstrated their interdependence to drive a robust antitumor response. Furthermore, V937 treatment of the co-culture increased both ICAM-1 and CVA21/V937 in the CRC-2 organoids, but not in the PBMCs. Therefore, the cross-talk appeared to be bidirectional. It is crucial to highlight that potentially V937 treatment may increase

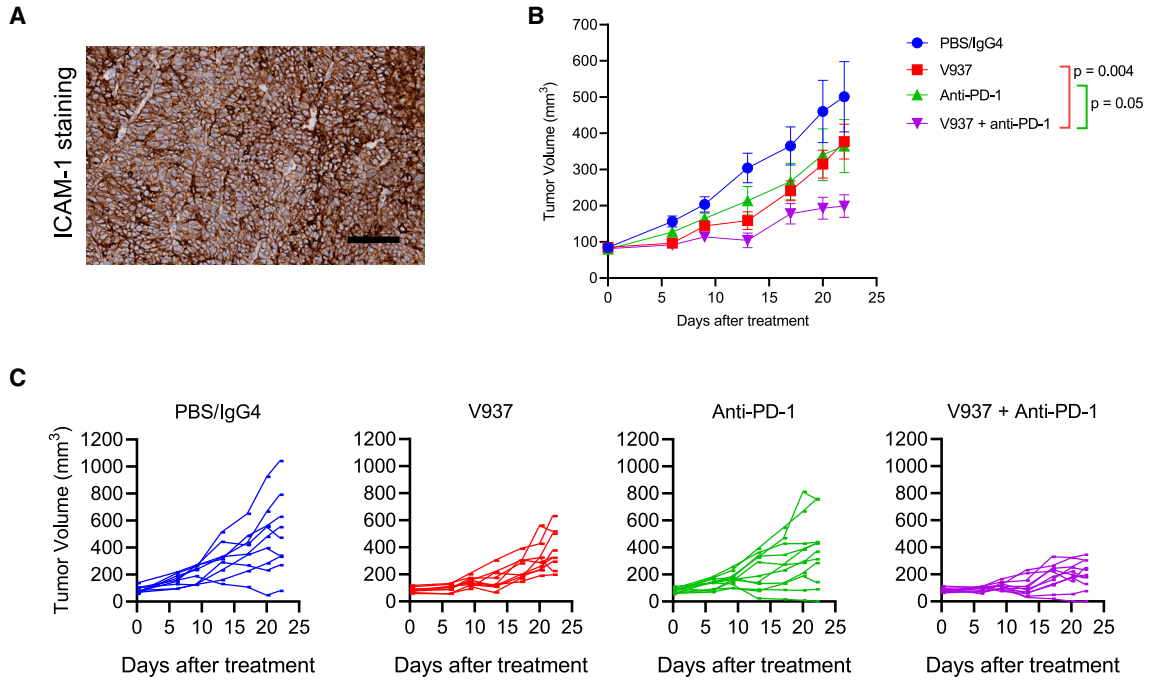


**Figure 7. Intratumoral V937 in combination with pembrolizumab reduced CRC-2 organoid burden in humanized mice**

CRC-2 organoids ($2 \times 10^6$ cells) in 1:1 suspension with Matrigel were subcutaneously injected into the right flanks of 40 female, 20-week-old CD34+ humanized NSG mice (The Jackson Laboratory). (A) IHC analysis of human ICAM-1 on CRC-2 tumors harvested 42 days following implant is shown. Scale bar, 100 μm. (B) Dosing was initiated 2 weeks following implantation of the CRC-2 organoids when the mean tumor volume reached 80 $mm^3$. The 40 humanized mice engrafted with CD34+ cells from three immune donors were distributed among four groups: Group 1: PBS or human IgG4 isotype control (10 mg/kg) ($n$ = 9), Group 2: V937 ($10^8$ PFU) ($n$ = 11), Group 3: Pembrolizumab (10 mg/kg) ($n$ = 9), and Group 4: V937 ($10^8$ PFU) + pembrolizumab (10 mg/kg) ($n$ = 11). PBS and V937 were administered intratumorally on days 0, 2, 4, 6, 13, 17, and 20, and isotype control or pembrolizumab were administered intraperitoneally on days 0, 7, and 14. Mean tumor volumes ± standard error of the mean is shown. (C) Individual tumor growth curves for each animal in the four groups are shown.

ICAM-1 expression on tumor cells, and in turn increase V937 infection and oncolysis of tumor cells.

Various cytokines, including IFN-γ, TNF-α, IL-1β, and IL-6, have been shown to increase ICAM-1 expression on various tumor types including squamous cell carcinoma, renal cell carcinoma, and breast carcinoma.[35,37,38] V937 treatment of the co-culture of HCC cell lines, CRC cell lines, and CRC organoids with PBMCs consistently induced IFN-γ. Here, we showed that recombinant IFN-γ induced dose-dependent ICAM-1 expression on the CRC cell line WIDR. Moreover, addition of IFN-γ with V937 drastically increased oncolysis, highlighted the importance of IFN-γ in mediating ICAM-1 expression of the cancer cells and played an essential role in the immune-tumor cross-talk upon V937 treatment. As induction of IFN-γ is a hallmark of PD-1 blockade, we assessed whether cross-linking CD3 with anti-PD-1 pembrolizumab mimics the effects of recombinant IFN-γ in the co-culture of either CRC cell lines or organoids with PBMCs. We showed that activation of T cells with anti-CD3 mAb in combination with pembrolizumab sensitized both COLO205 cells and CRC-3 organoids to V937-induced oncolysis. Last, we showed that intratumoral administration of V937 in combination with pembrolizumab significantly reduced the tumor burden of subcutaneous CRC-2 organoids in CD34+ humanized NSG mice.

Our study highlights the importance of cell models to evaluate tumor and immune cell interaction using both cancer cell lines and relevant organoid models. However, a few limitations of the models used in this study are worth mentioning, including the co-culture models with allogeneic donor PBMCs. In addition, the non-contact co-culture system did not fully capture the tumor microenvironment. For future studies, it would be interesting to determine the effect of the stroma or other microenvironment effects, such as hypoxia, in the co-culture system. Moreover, in the present study, we have yet to explore the role of different cytokines and chemokines beyond IFN-γ in mediating this immune-tumor cross-talk. A combination of cytokines rather than specific secreted factors will likely work together to induce the optimal tumor response.

Silk et al.[20] reported that in the Phase 1b CAPRA single-arm trial of intratumoral V937 in combination with pembrolizumab in patients with advanced melanoma, the responses were associated with increased serum CXCL10 (IP-10) and CCL22, suggesting viral replication contributes to antitumor immunity and occurred even in

patients without a typical "immune-active" microenvironment. These findings further support the model that V937 in combination with PD-1 blockade may induce significant antitumor immunity in immunologically quiescent tumor types, which may have lower ICAM-1 expression on tumor cells and lower baseline T cell infiltrates in the tumors. The data in the present study show mechanistically how V937 and pembrolizumab may act in synergy with V937-induced oncolysis augmenting the activity of pembrolizumab and pembrolizumab potentiating V937-induced oncolysis. V937 represents a potential versatile, immunotherapeutic modality to combine with PD-1 blockade for the treatment of immunologically quiescent tumors.

## MATERIALS AND METHODS

### TCGA and published study dataset analysis

The TCGA database (https://portal.gdc.cancer.gov/) was used for analysis of clinical samples. Spearman correlation was used to determine the correlation coefficient between indicated gene expression.

### V937 production

V937 was produced and purified at Merck & Co., Vaccine Process Research & Development, Kenilworth, New Jersey. In brief, V937 was produced from infected MRC-5 (derived from ECACC 06072101) cell culture using a virus seed derived from a CVA21 Kuykendall prototype strain (ATCC VR-850). Lysates were harvested and clarified through depth filters and purified across an affinity chromatography and two polishing ion-exchange chromatography steps and purified V937 was exchanged into a stabilizing buffer and passed through a 0.2-μm filter. PFUs of V937 lots were determined by standard plaque assay on human melanoma Mel624 or SKMEL28 cell lines. MOI is defined as the ratio of viral particles (PFUs) to number of cells.

### Primary human tissue, patient-derived organoids, and cell lines

The melanoma ($n = 93$), HCC ($n = 63$), and CRC ($n = 93$) tissues that were evaluated by IHC for ICAM-1 expression were commercially sourced, FFPE specimens from the Merck Research Laboratories, South San Francisco tissue bank.

Organoid cultures generated from primary normal colon or colorectal tumor tissues were obtained from surgically resected samples with informed consent from commercial sources (MT group, Discovery Life Sciences, Tissue Solutions). The characterization of tissue specimens as normal colon or colorectal cancer was confirmed by histopathological evaluation of H&E stains by a pathologist. One normal colorectal organoid line (NC-1) and CRC organoid lines (CRC-2 and CRC-3) were generated by 3D culturing of dissociated tissue.[33] CRC-3 was classified as infiltrative colonic adenocarcinoma, grade 3 (poorly differentiated/high grade) with carcinoma that invades muscularis propria based on pathology report. CRC-2 was classified as poorly differentiated high-grade adenocarcinoma based on tumor histology generated from CRC-2 organoids. The organoids developed by self-organization, and are mainly composed of adenocarcinoma epithelial cells and adult stem cells that are tissue-specific.[39] The fresh tissue was minced by a scalpel and embedded in Cultrex RGF BME Type R1 (Trevigen) with organoid medium consisting of 50% R-spondin, Noggin, and Wnt3a conditioned medium (from L-WRN cells, CRL-3276, ATCC), and completed with 50% advanced DMEM/F12 supplemented with penicillin/streptomycin, 10 mM HEPES, Glutamax (all from Lonza), Primocin (Invivogen), 1x B27 (Gibco), 1.25 mM N-Acetyl Cysteine (Sigma), 50 ng/mL human EGF (Peprotech), 10 μM Y-27632, 500 nM A83–01, 3 μM SB202190 (all from Selleck). For the culture of normal organoids, 25% of the Wnt3a conditioned medium (L-Wnt3a cells, CRL-2647, ATCC) was added in addition to the complete organoid medium described above. For terminal experiments with V937 treatment, intact CRC organoids were harvested and cultured in the organoid medium without ECM to allow V937 to infect the cancer cells.

All human cell lines were purchased from ATCC and cultured in DMEM or RPMI with 10% FBS supplemented with penicillin/streptomycin, 10 mM HEPES, and Glutamax at 37°C with 5% $CO_2$.

### Antibodies

Human IgG4 S228P isotype control (Lot 60AGK), anti-PD-1 hIgG4 S228P Pembrolizumab (Lot 30ADQ) were generated at Merck Research Laboratories. Anti-CD3 mAb (clone OKT3, #170-076-124) suitable for *ex vivo* T cell activation is from Miltenyl Biotec.

### Non-contact co-culture of tumor cells and PBMCs

In the co-culture system, human tumor cell lines or organoids were seeded in the lower chamber of a six-well plate and $2 \times 10^6$ healthy donor PBMCs (Stem Cell Technologies, 70025.2) were seeded in the top chamber of a transwell (Corning, 07-200-156) with RPMI (Gibco, 2156000) supplemented with Glutamine, HEPES, and 10% heat-inactivated FBS (Gibco, 26140-079). For organoid co-culture, organoids were extracted from Cultrex matrigel by Cultrex Organoid Harvesting Solution (Catalog # 3700-100-01). V937 was added to the bottom of the chamber. V937 is approximately 28 nm and can pass from the lower chamber to the upper chamber through the 0.4-μm pores of the insert. In some experiments, recombinant human IFN-γ protein was used (R&D systems, 285-IF). Following 48 or 72 h of treatment, the cells and culture media were harvested and stored at −80°C prior to processing and analysis.

### Cytokine/chemokine quantification assay

The concentrations of cytokines and chemokines were assessed by V-PLEX Proinflammatory Panel 1 Human Kit, V-PLEX Chemokine Panel 1 Human Kit (K15049D), U-PLEX Interferon Combo kit (K15094K), and V-PLEX Chemokine Panel 1 Human Kit (K15047D) from Meso Scale Discovery. The kits utilize multiplexed electrochemiluminescence, and light intensity was measured by SECTOR Imager S 600. The assays were performed according to the manufacturer's protocol.

### Flow cytometry analysis

Isolated cells were fixed for 30 min in fixable viability dye (eBioscience, 65-0866-14) in PBS, washed with FACS buffer (PBS/2% FBS/2 mM EDTA) and stained with either PE anti-human ICAM-1

**Table 1. List of primer assay used for RNA expression analysis**

| Common ID | Assay # | Common ID | Assay # |
|---|---|---|---|
| ACTA2 | Hs00426835_g1 | IL27 | Hs00377366_m1 |
| AIM2 | Hs00915710_m1 | IL33 | Hs00369211_m1 |
| ALPI | Hs00357579_g1 | IL6 | Hs00985639_m1 |
| ANPEP | Hs00174265_m1 | IL6RA | Hs01075666_m1 |
| APC | Hs00181051_m1 | IL7 | Hs00174202_m1 |
| APOBEC3G | Hs00222415_m1 | IL7R | Hs00233682_m1 |
| ASCL2 | Hs00270888_s1 | IRF3 | Hs01547283_m1 |
| ATG3 | Hs00223937_m1 | IRF4 | Hs00180031_m1 |
| ATG5 | Hs00169468_m1 | IRF7 | Hs01014809_g1 |
| AXIN2 | Hs00610344_m1 | ISG15 | Hs00192713_m1 |
| B2M | Hs99999907_m1 | JAG1 | Hs00164982_m1 |
| BAX | Hs00180269_m1 | JUN | Hs01103582_s1 |
| BMI1 | Hs00995536_m1 | KIT | Hs00174029_m1 |
| BMP4 | Hs00370078_m1 | KRT18 | Hs01941416_g1 |
| CARD9 | Hs00364485_m1 | KRT20 | Hs00300643_m1 |
| CASP10 | Hs01017899_m1 | LAG3 | Hs00158563_m1 |
| CASP8 | Hs01018151_m1 | LGR5 | Hs00969420_m1 |
| CCL3 | Hs00234142_m1 | LOX | Hs00942482_g1 |
| CCL5 | Hs00174575_m1 | MAP2K1 | Hs00983247_g1 |
| PROM1 | Hs00195682_m1 | MAP2K3 | Hs00177127_m1 |
| CD27 | Hs00386811_m1 | MAP3K1 | Hs00394890_m1 |
| CD276 | Hs00987207_m1 | MAP3K7 | Hs01105682_m1 |
| CD40 | Hs00374176_m1 | MAPK1 | Hs00177066_m1 |
| CD44 | Hs00153304_m1 | MAPK14 | Hs01051152_m1 |
| CD55 | Hs00167090_m1 | MAPK3 | Hs00946872_m1 |
| NT5E | Hs01573923_m1 | MAPK8 | Hs01548508_m1 |
| CD80 | Hs00175478_m1 | MCM4 | Hs00381533_m1 |
| CD8A | Hs00233520_m1 | MCM6 | Hs00195504_m1 |
| THY1 | Hs00174816_m1 | MEFV | Hs00925524_m1 |
| CDKN1A | Hs00355782_m1 | MICA | Hs00741286_m1 |
| CEACAM16 | Hs00975061_m1 | MICB | Hs00746491_s1 |
| CEACAM7 | Hs00185152_m1 | MKI67 | Hs01032443_m1 |
| CHUK | Hs00989502_m1 | MUC1 | Hs00159357_m1 |
| CMKLR1 | Hs01081979_s1 | MUC2 | Hs03005103_g1 |
| CTSB | Hs00164368_m1 | MX1 | Hs00182073_m1 |
| CTSL | Hs00266474_m1 | MYC | Hs00153408_m1 |
| CTSL1 | Hs00175407_m1 | MYD88 | Hs01573837_g1 |
| CVA21 | CVA21_Custom | NANOG | Hs02387400_g1 |
| CX3CL1 | Hs00171086_m1 | NFKB1 | Hs00765730_m1 |
| CXCL10 | Hs00171042_m1 | NFKBIA | Hs00355671_g1 |
| CXCL11 | Hs00171138_m1 | NKG7 | Hs01120688_g1 |
| CXCL12 | Hs00171022_m1 | NLRP3 | Hs00918082_m1 |
| CXCL13 | Hs00757930_m1 | NOD2 | Hs00223394_m1 |
| CXCL2 | Hs00601975_m1 | PMAIP1 | Hs00560402_m1 |
| CXCL3 | Hs00171061_m1 | OAS2 | Hs00942643_m1 |
| PF4 | Hs00427220_g1 | PDCD1 | Hs00169472_m1 |
| CXCL5 | Hs00171085_m1 | PDGFA | Hs00236997_m1 |
| CXCL6 | Hs00237017_m1 | PDGFRA | Hs00998018_m1 |
| CXCL8 | Hs00174103_m1 | PDGFRB | Hs01019589_m1 |
| CXCL9 | Hs00171065_m1 | CD274 | Hs00204257_m1 |
| CXCR1 | Hs00174146_m1 | PDCD1LG2 | Hs00228839_m1 |
| CXCR3 | Hs01847760_s1 | PDPN | Hs00366766_m1 |
| CXCR4 | Hs00607978_s1 | PIN1 | Hs01598308_m1 |
| CXCR5 | Hs99999128_s1 | POSTN | Hs01566747_m1 |
| CXCR6 | Hs00174843_m1 | PRF1 | Hs00169473_m1 |
| CYLD | Hs00211000_m1 | PSMB10 | Hs00160620_m1 |
| DDX3X | Hs00606179_m1 | PSTPIP1 | Hs00182777_m1 |
| DDX58 | Hs00204833_m1 | PTK6 | Hs00966641_m1 |
| FGFR2 | Hs01552920_m1 | BBC3 | Hs00248075_m1 |
| FZD3 | Hs00184043_m1 | PYCARD | Hs00203118_m1 |
| GADD45A | Hs00169255_m1 | RELA | Hs00153294_m1 |
| GZMA | Hs00196206_m1 | RIPK1 | Hs00169407_m1 |
| GZMB | Hs00188051_m1 | S100A4 | Hs00243202_m1 |
| HLA-A | Hs01058806_g1 | SOX17 | Hs00751752_s1 |
| HLA-B | Hs00818803_g1 | STAT1 | Hs00234829_m1 |
| HLA-C | Hs03044135_m1 | STAT3 | Hs01051722_s1 |
| HLA-DQA1 | Hs03007426_mH | TAP1 | Hs00388675_m1 |
| HLA-DRB1 | Hs99999917_m1 | TAP2 | Hs00241060_m1 |
| HLA-E | Hs03045171_m1 | TBK1 | Hs00179410_m1 |
| HSP90AA1 | Hs00743767_sH | TEK | Hs00945146_m1 |
| ICAM1 | Hs00164932_m1 | TGFB1 | Hs00171257_m1 |
| IDO1 | Hs00158027_m1 | TGFB2 | Hs00234244_m1 |
| IFIH1 | Hs00223420_m1 | TGFB3 | Hs00234245_m1 |
| IFNA1 | Hs00855471_g1 | TIGIT | Hs00545087_m1 |
| IFNA2 | Hs00265051_s1 | TIMP1 | Hs00171558_m1 |
| IFNAR1 | Hs01066116_m1 | TIMP2 | Hs00234278_m1 |
| IFNB1 | Hs01077958_s1 | TLR3 | Hs01551078_m1 |
| IFNG | Hs00989291_m1 | TLR7 | Hs01933259_s1 |
| IHH | Hs01081801_m1 | TLR8 | Hs00607866_mH |
| IKBKB | Hs00233287_m1 | TLR9 | Hs00370913_s1 |
| IL10 | Hs00174086_m1 | TNF | Hs00174128_m1 |
| IL12A | Hs01073447_m1 | TNFRSF10A | Hs00269492_m1 |
| IL12B | Hs01011518_m1 | CCND1 | Hs00765553_m1 |
| IL15 | Hs00174106_m1 | TNFRSF9 | Hs00155512_m1 |
| IL18 | Hs01038788_m1 | TNFSF8 | Hs00174286_m1 |
| IL1A | Hs00174092_m1 | TRADD | Hs00601065_g1 |
| IL1B | Hs01555410_m1 | TRAF3 | Hs00974570_m1 |
| IL2 | Hs00174114_m1 | TRAF6 | Hs00270336_m1 |

(*Continued*)

**Table 1. *Continued***

(*Continued on next page*)

**Table 1. *Continued***

| Common ID | Assay # | Common ID | Assay # |
|---|---|---|---|
| IL21 | Hs00222327_m1 | TRIM25 | Hs01116121_m1 |
| IL21R | Hs00222310_m1 | VIL1 | Hs01031739_m1 |
| IL22 | Hs01574152_g1 | WNT2 | Hs00608224_m1 |
| IL23A | Hs00372324_m1 | WNT3A | Hs00263977_m1 |
| | | UBB | Hs00430290_m1 |

(Biolegend, 353105) or PE Mouse IgG1 isotype (Biolegend, 400113) for 30 min on ice. The cells were analyzed on LSRFortessa flow cytometer (BD Biosciences). Data were acquired using the FACS DIVA software (BD Biosciences). All flow cytometry data were analyzed with FlowJo (TreeStar Software).

### Apoptotic cell death analysis

Apoptotic cell death was quantified by Cell Death Detection Plus ELISA (Roche) or Incucyte S3 using Incucyte Annexin V Red dye or Cytotox Green dye (Essence BioScience, Hertfordshire, United Kingdom). The assays were performed according to the manufacturer's protocol.

### CellTiter-Glo Luminescent cell viability assay

CellTiter-Glo Luminescent Cell Viability Assay (Promega, G7571) was used to determine cell viability based on quantitation of ATP. The assay was performed according to the manufacturer's protocol.

### RNA expression analysis

For real-time PCR analysis, total RNA was isolated from cells using Arcturus PicoPure RNA Isolation method, according to the manufacturer's protocol (Thermo Fisher Scientific). DNase-treated total RNA was reverse transcribed using QuantiTect Reverse Transcription (Qiagen) according to the manufacturer's instructions. Primers were obtained commercially from Thermo Fisher Scientific. Primer assay IDs are listed in Table 1. Gene-specific preamplification was done per Standard Biotools Biomark manufacturer's instructions (Standard Biotools). Real-time quantitative PCR was performed on the Fluidigm Biomark using 20X Taqman primer assays (Thermo Fisher Scientific) with TaqMan Fast Universal PCR Master Mix with UNG. Samples and primers were run on a 96.96 Dynamic Array per manufacturer's instructions (Standard Biotools). Ubiquitin levels were measured in a separate reaction and used to normalize the data by the Δ Ct method. Using the mean-cycle threshold value for ubiquitin and the gene of interest for each sample, the Equation 1.8 ^ (Ct ubiquitin minus Ct gene of interest) $\times$ $10^4$ was used to obtain the normalized values.

### Immunohistochemistry

IHC for ICAM-1 was conducted on 5-μm sections of FFPE tissue. In brief, tissue sections were deparaffinized and rehydrated with serial passage through changes of xylene and graded ethanols. All slides were subjected to heat-induced epitope retrieval in Envision FLEX Target Retrieval Solution, High pH (Dako Corporation, Carpinteria, CA) in a PT Link unit (Dako). Endogenous peroxidase in tissues was blocked by incubation of slides in 3% hydrogen peroxide solution before incubation with primary antibody (anti-ICAM-1 clone E3Q9N, Cell Signaling Technology, Danvers, MA) for 60 min. Antigen-antibody binding was visualized with the FLEX + polymer system (Dako) and application of 3,3′ diaminobenzidine chromogen (Dako). Stained slides were counterstained with hematoxylin and coverslipped for review and scoring. Scoring was conducted by a pathologist using a semiquantitative scale of 0–5, in which positive tumor and immune cell frequency within the tumor region was grouped into the following categories: 0 indicates negative, 1 indicates rare, 2 indicates low, 3 indicates moderate, 4 indicates high, and 5 indicates very high.

### Humanized mice study

All mouse experiments were conducted according to protocols approved by the Institutional Animal Care and Use Committee at Merck Research Labs, South San Francisco, CA. Forty 20-week-old CD34+ humanized NSG mice (The Jackson Laboratory) which were engrafted with human cord blood derived CD34+ cells from three immune donors, confirmed to have engraftment of >25% hu-CD45+ cells in the peripheral blood. CRC-2 organoids were cultured in organoid media for 1 week, and the organoids were harvested with TrypLE Express (Thermo, 12604013) to obtain a single cell suspension. Cells were added to the solution of Matrigel (Corning, 354263) diluted 1:3 in PBS; 100 μL of the cell mixture with approximately 2 $\times$ $10^6$ live cells were implanted subcutaneously onto the right flank of the 40 CD34+ humanized NSG mice using 26-gauge syringe needles (BD, Cat# 305111). Treatment was initiated when the mean tumor volume reached 80 $mm^3$, 2 weeks following implant of CRC-2 organoids. The mice, representing three immune donors, were distributed across four groups: Group 1: PBS/10 mg/kg isotype hIgG4; Group 2: $10^8$ PFU V937; Group 3: 10 mg/kg anti-PD-1 pembrolizumab; Group 4: $10^8$ PFU V937 and 10 mg/kg pembrolizumab. PBS and V937 were administered intratumorally on days 0, 2, 4, 6, 13, 17, and 20, and isotype control mAb or pembrolizumab were administered intraperitoneally on days 0, 7, and 14. Tumor volumes ($mm^3$) were calculated using the following formula: (length $\times$ $width^2$)/2.

### Statistical analysis

Statistical analysis was performed using Excel (Microsoft) and GraphPad Prism 6 (Graphpad software, Inc) to determine the statistical significance of differences between means. Unless otherwise specified, Student's t test was used for calculating $p$ value.

## DATA AND CODE AVAILABILITY

All data generated or analyzed during this study are included in this article and supplemental information.

## SUPPLEMENTAL INFORMATION

Supplemental information can be found online at https://doi.org/10.1016/j.omton.2024.200807.

## ACKNOWLEDGMENTS

We would like to thank members of South San Francisco Discovery Oncology Department at Merck for helpful comments on the manuscript. The authors acknowledge support from the Merck Research Laboratories Postdoctoral Research Program.

## AUTHOR CONTRIBUTIONS

T.T., J.C.W., U.P., and A.A.C. conceptualized and designed the study. T.T., J.C.W., U.P., and S.S. developed methodology. T.T., J.C.W., J.G., and M.S. generated and analyzed data. T.T., U.P., J.C.W., and W.M.B. performed data analysis and interpretation. T.T., J.C.W., U.P., and A.A.C. wrote and revised the manuscript. S.S. supervised the study.

## DECLARATION OF INTERESTS

J.G., J.H.Y., W.M.B., and S.S. are employees at Merck & Co. J.C.W. is an employee at ALX Oncology, T.T. is an employee at Novartis, L.A. is an employee at Denali Therapeutics, and U.P. is an employee at Inverna.

## REFERENCES

1. Ribas, A., and Wolchok, J.D. (2018). Cancer immunotherapy using checkpoint blockade. Science *359*, 1350–1355. https://doi.org/10.1126/science.aar4060.

2. Tumeh, P.C., Harview, C.L., Yearley, J.H., Shintaku, I.P., Taylor, E.J.M., Robert, L., Chmielowski, B., Spasic, M., Henry, G., Ciobanu, V., et al. (2014). PD-1 blockade induces responses by inhibiting adaptive immune resistance. Nature *515*, 568–571. https://doi.org/10.1038/nature13954.

3. Chen, P.L., Roh, W., Reuben, A., Cooper, Z.A., Spencer, C.N., Prieto, P.A., Miller, J.P., Bassett, R.L., Gopalakrishnan, V., Wani, K., et al. (2016). Analysis of Immune Signatures in Longitudinal Tumor Samples Yields Insight into Biomarkers of Response and Mechanisms of Resistance to Immune Checkpoint Blockade. Cancer Discov. *6*, 827–837. https://doi.org/10.1158/2159-8290.CD-15-1545.

4. Cristescu, R., Mogg, R., Ayers, M., Albright, A., Murphy, E., Yearley, J., Sher, X., Liu, X.Q., Lu, H., Nebozhyn, M., et al. (2018). Pan-tumor genomic biomarkers for PD-1 checkpoint blockade-based immunotherapy. Science *362*, eaar3593. https://doi.org/10.1126/science.aar3593.

5. Kaufman, H.L., Kohlhapp, F.J., and Zloza, A. (2015). Oncolytic viruses: a new class of immunotherapy drugs. Nat. Rev. Drug Discov. *14*, 642–662. https://doi.org/10.1038/nrd4663.

6. Keller, B.A., and Bell, J.C. (2016). Oncolytic viruses-immunotherapeutics on the rise. J. Mol. Med. *94*, 979–991. https://doi.org/10.1007/s00109-016-1453-9.

7. Sivanandam, V., LaRocca, C.J., Chen, N.G., Fong, Y., and Warner, S.G. (2019). Oncolytic Viruses and Immune Checkpoint Inhibition: The Best of Both Worlds. Mol. Ther. Oncolytics *13*, 93–106. https://doi.org/10.1016/j.omto.2019.04.003.

8. Zheng, M., Huang, J., Tong, A., and Yang, H. (2019). Oncolytic Viruses for Cancer Therapy: Barriers and Recent Advances. Mol. Ther. Oncolytics *15*, 234–247. https://doi.org/10.1016/j.omto.2019.10.007.

9. Bommareddy, P.K., Shettigar, M., and Kaufman, H.L. (2018). Author Correction: Integrating oncolytic viruses in combination cancer immunotherapy. Nat. Rev. Immunol. *18*, 536. https://doi.org/10.1038/s41577-018-0031-5.

10. Lemos de Matos, A., Franco, L.S., and McFadden, G. (2020). Oncolytic Viruses and the Immune System: The Dynamic Duo. Mol. Ther. Methods Clin. Dev. *17*, 349–358. https://doi.org/10.1016/j.omtm.2020.01.001.

11. Davola, M.E., and Mossman, K.L. (2019). Oncolytic viruses: how "lytic" must they be for therapeutic efficacy? Oncoimmunology *8*, e1581528. https://doi.org/10.1080/2162402X.2019.1596006.

12. Leddon, J.L., Chen, C.Y., Currier, M.A., Wang, P.Y., Jung, F.A., Denton, N.L., Cripe, K.M., Haworth, K.B., Arnold, M.A., Gross, A.C., et al. (2015). Oncolytic HSV virotherapy in murine sarcomas differentially triggers an antitumor T-cell response in the absence of virus permissivity. Mol. Ther. Oncolytics *1*, 14010. https://doi.org/10.1038/mto.2014.10.

13. Workenhe, S.T., Simmons, G., Pol, J.G., Lichty, B.D., Halford, W.P., and Mossman, K.L. (2014). Immunogenic HSV-mediated oncolysis shapes the antitumor immune response and contributes to therapeutic efficacy. Mol. Ther. *22*, 123–131. https://doi.org/10.1038/mt.2013.238.

14. Rameshbabu, S., Labadie, B.W., Argulian, A., and Patnaik, A. (2021). Targeting Innate Immunity in Cancer Therapy. Vaccines (Basel) *9*, 138. https://doi.org/10.3390/vaccines9020138.

15. Andtbacka, R.H.I., Kaufman, H.L., Collichio, F., Amatruda, T., Senzer, N., Chesney, J., Delman, K.A., Spitler, L.E., Puzanov, I., Agarwala, S.S., et al. (2015). Talimogene Laherparepvec Improves Durable Response Rate in Patients With Advanced Melanoma. J. Clin. Oncol. *33*, 2780–2788. https://doi.org/10.1200/JCO.2014.58.3377.

16. Shafren, D.R., Dorahy, D.J., Ingham, R.A., Burns, G.F., and Barry, R.D. (1997). Coxsackievirus A21 binds to decay-accelerating factor but requires intercellular adhesion molecule 1 for cell entry. J. Virol. *71*, 4736–4743. https://doi.org/10.1128/JVI.71.6.4736-4743.1997.

17. Müller, L.M.E., Holmes, M., Michael, J.L., Scott, G.B., West, E.J., Scott, K.J., Parrish, C., Hall, K., Stäble, S., Jennings, V.A., et al. (2019). Plasmacytoid dendritic cells orchestrate innate and adaptive anti-tumor immunity induced by oncolytic coxsackievirus A21. J. Immunother. Cancer *7*, 164. https://doi.org/10.1186/s40425-019-0632-y.

18. Shafren, D.R., Au, G.G., Nguyen, T., Newcombe, N.G., Haley, E.S., Beagley, L., Johansson, E.S., Hersey, P., and Barry, R.D. (2004). Systemic therapy of malignant human melanoma tumors by a common cold-producing enterovirus, coxsackievirus a21. Clin. Cancer Res. *10*, 53–60. https://doi.org/10.1158/1078-0432.ccr-0690-3.

19. Andtbacka, R.H.I., Curti, B., Daniels, G.A., Hallmeyer, S., Whitman, E.D., Lutzky, J., Spitler, L.E., Zhou, K., Bommareddy, P.K., Grose, M., et al. (2021). Clinical Responses of Oncolytic Coxsackievirus A21 (V937) in Patients With Unresectable Melanoma. J. Clin. Oncol. *39*, 3829–3838. https://doi.org/10.1200/JCO.20.03246.

20. Silk, A.W., O'Day, S.J., Kaufman, H.L., Bryan, J., Norrell, J.T., Imbergamo, C., Portal, D., Zambrano-Acosta, E., Palmeri, M., Fein, S., et al. (2022). A phase 1b single-arm trial of intratumoral oncolytic virus V937 in combination with pembrolizumab in patients with advanced melanoma: results from the CAPRA study. Cancer Immunol. Immunother. *72*, 1405–1415. https://doi.org/10.1007/s00262-022-03314-1.

21. Raimondi, G., Mato-Berciano, A., Pascual-Sabater, S., Rovira-Rigau, M., Cuatrecasas, M., Fondevila, C., Sánchez-Cabús, S., Begthel, H., Boj, S.F., Clevers, H., and Fillat, C. (2020). Patient-derived pancreatic tumour organoids identify therapeutic responses to oncolytic adenoviruses. EBioMedicine *56*, 102786. https://doi.org/10.1016/j.ebiom.2020.102786.

22. Hamdan, F., Ylösmäki, E., Chiaro, J., Giannoula, Y., Long, M., Fusciello, M., Feola, S., Martins, B., Feodoroff, M., Antignani, G., et al. (2021). Novel oncolytic adenovirus expressing enhanced cross-hybrid IgGA Fc PD-L1 inhibitor activates multiple immune effector populations leading to enhanced tumor killing *in vitro*, *in vivo* and with patient-derived tumor organoids. J. Immunother. Cancer *9*, e003000. https://doi.org/10.1136/jitc-2021-003000.

23. Carter, M.E., Hartkopf, A.D., Wagner, A., Volmer, L.L., Brucker, S.Y., Berchtold, S., Lauer, U.M., and Koch, A. (2022). A Three-Dimensional Organoid Model of Primary Breast Cancer to Investigate the Effects of Oncolytic Virotherapy. Front. Mol. Biosci. *9*, 826302. https://doi.org/10.3389/fmolb.2022.826302.

24. Del Bufalo, F., Manzo, T., Hoyos, V., Yagyu, S., Caruana, I., Jacot, J., Benavides, O., Rosen, D., and Brenner, M.K. (2016). 3D modeling of human cancer: A PEG-fibrin hydrogel system to study the role of tumor microenvironment and recapitulate the *in vivo* effect of oncolytic adenovirus. Biomaterials *84*, 76–85. https://doi.org/10.1016/j.biomaterials.2016.01.030.

25. Lim, E.J., Kang, J.H., Kim, Y.J., Kim, S., and Lee, S.J. (2022). ICAM-1 promotes cancer progression by regulating SRC activity as an adapter protein in colorectal cancer. Cell Death Dis. *13*, 417. https://doi.org/10.1038/s41419-022-04862-1.

26. Muthuswamy, S.K., and Xue, B. (2012). Cell Polarity As A Regulator of Cancer Cell Behavior Plasticity. Annu. Rev. Cell Dev. Biol. *28*, 599–625. https://doi.org/10.1146/annurev-cellbio-092910-154244.

27. Möst, J., Schwaeble, W., Drach, J., Sommerauer, A., and Dierich, M.P. (1992). Regulation of the expression of ICAM-1 on human monocytes and monocytic tumor cell lines. J. Immunol. *148*, 1635–1642.

28. Tran, T.Q., Hanse, E.A., Habowski, A.N., Li, H., Ishak Gabra, M.B., Yang, Y., Lowman, X.H., Ooi, A.M., Liao, S.Y., Edwards, R.A., et al. (2020). alpha-Ketoglutarate attenuates Wnt signaling and drives differentiation in colorectal cancer. Nat. Cancer *1*, 345–358. https://doi.org/10.1038/s43018-020-0035-5.

29. van de Wetering, M., Francies, H.E., Francis, J.M., Bounova, G., Iorio, F., Pronk, A., van Houdt, W., van Gorp, J., Taylor-Weiner, A., Kester, L., et al. (2015). Prospective derivation of a living organoid biobank of colorectal cancer patients. Cell *161*, 933–945. https://doi.org/10.1016/j.cell.2015.03.053.

30. Zhou, Z., Cong, L., and Cong, X. (2021). Patient-Derived Organoids in Precision Medicine: Drug Screening, Organoid-on-a-Chip and Living Organoid Biobank. Front. Oncol. *11*, 762184. https://doi.org/10.3389/fonc.2021.762184.

31. Ooft, S.N., Weeber, F., Dijkstra, K.K., McLean, C.M., Kaing, S., van Werkhoven, E., Schipper, L., Hoes, L., Vis, D.J., van de Haar, J., et al. (2019). Patient-derived organoids can predict response to chemotherapy in metastatic colorectal cancer patients. Sci. Transl. Med. *11*, eaay2574. https://doi.org/10.1126/scitranslmed.aay2574.

32. Vlachogiannis, G., Hedayat, S., Vatsiou, A., Jamin, Y., Fernández-Mateos, J., Khan, K., Lampis, A., Eason, K., Huntingford, I., Burke, R., et al. (2018). Patient-derived organoids model treatment response of metastatic gastrointestinal cancers. Science *359*, 920–926. https://doi.org/10.1126/science.aao2774.

33. Sato, T., Vries, R.G., Snippert, H.J., van de Wetering, M., Barker, N., Stange, D.E., van Es, J.H., Abo, A., Kujala, P., Peters, P.J., and Clevers, H. (2009). Single Lgr5 stem cells build crypt-villus structures *in vitro* without a mesenchymal niche. Nature *459*, 262–265. https://doi.org/10.1038/nature07935.

34. Au, G.G., Lincz, L.F., Enno, A., and Shafren, D.R. (2007). Oncolytic Coxsackievirus A21 as a novel therapy for multiple myeloma. Br. J. Haematol. *137*, 133–141. https://doi.org/10.1111/j.1365-2141.2007.06550.x.

35. Scher, R.L., Koch, W.M., and Richtsmeier, W.J. (1993). Induction of the intercellular adhesion molecule (ICAM-1) on squamous cell carcinoma by interferon gamma. Arch. Otolaryngol. Head Neck Surg. *119*, 432–438. https://doi.org/10.1001/archotol.1993.01880160080012.

36. Rudin, C.M., Pandha, H.S., Zibelman, M., Akerley, W.L., Harrington, K.J., Day, D., Hill, A.G., O'Day, S.J., Clay, T.D., Wright, G.M., et al. (2023). Phase 1, open-label, dose-escalation study on the safety, pharmacokinetics, and preliminary efficacy of intravenous Coxsackievirus A21 (V937), with or without pembrolizumab, in patients with advanced solid tumors. J. Immunother. Cancer *11*, e005007. https://doi.org/10.1136/jitc-2022-005007.

37. Hutchins, D., and Steel, C.M. (1994). Regulation of ICAM-1 (CD54) expression in human breast cancer cell lines by interleukin 6 and fibroblast-derived factors. Int. J. Cancer *58*, 80–84. https://doi.org/10.1002/ijc.2910580114.

38. Tomita, Y., Nishiyama, T., Watanabe, H., Fujiwara, M., and Sato, S. (1990). Expression of intercellular adhesion molecule-1 (ICAM-1) on renal-cell cancer: possible significance in host immune responses. Int. J. Cancer *46*, 1001–1006. https://doi.org/10.1002/ijc.2910460609.

39. Porter, R.J., Murray, G.I., and McLean, M.H. (2020). Current concepts in tumour-derived organoids. Br. J. Cancer *123*, 1209–1218. https://doi.org/10.1038/s41416-020-0993-5.